

The physics and the structure of the quasar-driven outflow in Mrk 231

C. Cicone^{1,2}, C. Feruglio³, R. Maiolino^{1,2}, F. Fiore¹, E. Piconcelli^{1,4}, N. Menci¹, H. Aussel⁵, and E. Sturm⁶

¹ Cavendish Laboratory, University of Cambridge 19 J. J. Thomson Avenue, Cambridge CB3 0HE, UK
e-mail: c.cicone@mrao.cam.ac.uk

² INAF - Osservatorio Astronomico di Roma (OAR), via Frascati 33, 00040 Monteporzio Catone, Italy

³ Institut de Radio Astronomie Millimétrique (IRAM), 300 rue de la Piscine, St. Martin d'Hères, France

⁴ XMM-Newton Science Operations Centre, ESA, P.O. Box 78, 28691 Villanueva de la Caada, Madrid, Spain

⁵ Laboratoire AIM, DSM/Irfu/Service d'Astrophysique, CEA Saclay, 91191 Gif-sur-Yvette, France

⁶ Max Planck Institute für Extraterrestrische Physik (MPE), Postfach 1312, D85741 Garching, Germany

Received ???; accepted ...

Abstract

Massive AGN-driven outflows are invoked by AGN-galaxy co-evolutionary models to suppress both star formation and black hole accretion. Massive molecular outflows have recently been revealed in some AGN hosts. However, the physical properties and structure of these AGN-driven molecular outflows are still poorly constrained. Here we present new IRAM PdBI observations of Mrk 231, the closest quasar known, targeting both the CO(1-0) and CO(2-1) transitions. We detect broad wings in both transitions, tracing a massive molecular outflow with velocities up to 800 km/s. The wings are spatially resolved at high significance level (5–11 σ), indicating that the molecular outflow extends on the kpc scale. The CO(2-1)/CO(1-0) ratio of the red broad wings is consistent with the ratio observed in the narrow core, while the blue broad wing is less excited than the core. The latter result suggests that quasar driven outflow models invoking shocks (which would predict higher gas excitation) are not appropriate to describe the bulk of the outflow in Mrk 231. However, we note that within the central 700 pc the CO(2-1)/CO(1-0) ratio of the red wing is slightly, but significantly, higher than in the line core, suggesting that shocks may play a role in the central region. We also find that the average size of the outflow anticorrelates with the critical density of the transition used as a wind tracer. This indicates that, although diffuse and dense clumps coexist in the outflowing gas, dense outflowing clouds have shorter lifetime and that they evaporate into the diffuse component along the outflow or, more simply, that diffuse clouds are more efficiently accelerated to larger distances by radiation pressure.

Key words. Galaxies: active – Galaxies: evolution – Galaxies: individual: Mrk 231 – quasars: general – Radio lines:ISM – ISM: molecules

1. Introduction

The ubiquitous discovery of “relic” supermassive black holes (SMBH) in local bulges and of the tight correlations between their masses and bulge properties (e.g. Ferrarese & Ford 2005; Marconi & Hunt 2003; Gültekin et al. 2009; and ref. therein) hints that the nuclear activity likely plays an important role in galaxy evolution. Recently, considerable attention has been drawn to powerful AGN-driven outflows as they might provide a very efficient mechanism enabling the nuclear activity occurring on sub-parsec scales to produce its influence upon the surrounding host galaxy. The effect of these AGN winds on the interstellar matter (ISM) in the galaxy is often referred to as “AGN feedback”. More specifically, AGN feedback is invoked by most of the current galaxy evolutionary models to explain the shortage of very massive galaxies in the local Universe, their red colors and low gas content, as well as the $M_{\text{BH}} - \sigma$ relation (e.g. Silk & Rees 1998, Fabian 1999, King & Pounds 2003; Fabian et al. 2006 Baldry et al. 2004; Granato et al. 2004; Di Matteo et al. 2005; Elvis 2006; Lapi et al. 2005; King 2005; Menci et al. 2006, 2008; Croton et al. 2006; Narayanan et al. 2008; Hopkins & Elvis 2010).

There are two possible “flavors” of AGN feedback: feedback associated with the “radio-mode” (Croton et al. 2006) and feedback associated with the “quasar-mode”. In this work we focus only on the second one, which is the impulsive feedback exerted by AGNs during their bright active phases. One of the most common scenarios in theoretical models of quasar-mode feedback is that nuclear fast winds, originated by the AGN radiation pressure, deposit the energy produced by the nuclear activity into the ISM, compressing the ISM into a shock wave (“blast wave”) that eventually blows the cold gas reservoir, available for both star formation and SMBH accretion, out of the host galaxy (Lapi et al. 2005; Menci et al. 2006, 2008; King 2010, Zubovas & King 2012). Models expect that such outflows may also include a significant molecular component (Zubovas & King 2012, Narayanan et al. 2008). If AGN-driven outflows can really expel large quantities of molecular gas (which constitutes the bulk of the ISM in the central regions and is the medium out of which stars form), then this would really be an effective mechanism to quench star formation in massive galaxies.

Major observational breakthroughs in this field have been recently obtained by revealing massive and energetic quasar

driven outflows in several galaxies, both locally and at high redshift (Fischer et al. 2010; Feruglio et al. 2010; Rupke & Veilleux 2011; Aalto et al. 2012; Sturm et al. 2011; Alatalo et al. 2011; Greene et al. 2011; Nesvadba et al. 2010, 2011; Alexander et al. 2010; Farrah et al. 2012; Cano-Díaz et al. 2012; Maiolino et al. 2012) (see also the recent review by Fabian 2012). Within this context, Mrk 231, the closest quasar known, is the object in which a massive quasar-driven outflow was first discovered and which has been studied in greater detail (Fischer et al. 2010; Feruglio et al. 2010; Rupke & Veilleux 2011, Aalto et al. 2012). Mrk 231 provides a unique, nearby laboratory for investigating AGN feedback, showing all of the typical features expected for a quasar transiting from the obscured, merger-driven and IR-luminous accretion phase, accompanied by strong circumnuclear star formation, to the unobscured, standard phase of 'blue' quasar (Lipari et al. 2009 and references therein), by expelling obscuring gas and dust. It is indeed the most luminous Ultra-Luminous Infrared Galaxy (ULIRG) in the local Universe (Sanders et al. 2003), with $L_{IR}(8-1000\mu\text{m}) = 1.33 \times 10^{46} \text{ erg s}^{-1}$, and it also hosts a very powerful ($L_{bol, AGN} = 1.1 \times 10^{46} \text{ erg s}^{-1}$; e.g., Rupke & Veilleux 2011), low-ionization broad absorption line (LoBAL) quasar (i.e. where the blue-shifted UV lines span velocities up to $\sim 8000 \text{ km s}^{-1}$). Boroson & Meyers (1992) argued that LoBAL quasars are young, heavily enshrouded AGNs, where the cocoon of gas and dust has a large covering factor, as supported by the results by Braito et al. (2004), who have found that Mrk 231 is a very obscured X-ray source with a column density of $N_H \approx 10^{24} \text{ cm}^{-2}$. Mrk 231 also shows a distorted optical morphology pointing to a host galaxy at an advanced stage of a merging process (Lipari et al. 2009). The circumnuclear starburst in this source is very young ($\lesssim 120 \text{ Myr}$), with an estimated star formation rate of $\text{SFR} \approx 200 \text{ M}_\odot \text{ yr}^{-1}$ (Taylor et al. 1999; Davies et al. 2004).

The Herschel-PACS spectrum of Mrk 231 has revealed the remarkable presence of a massive molecular outflow traced by prominent P-Cygni OH profiles at 65, 79, and 119 μm with velocity shifts of $\sim 1000 \text{ km s}^{-1}$ (Fischer et al. 2010). In Feruglio et al. (2010), we reported the detection of the molecular outflow through IRAM PdBI observations, which have revealed broad (FWZI $\sim 1500 \text{ km s}^{-1}$) wings of the CO(1-0) transition, and which are marginally resolved with an extension of about $\sim 1 \text{ kpc}$, yielding an estimated mass outflow rate of $\sim 700 \text{ M}_\odot \text{ yr}^{-1}$, i.e., far larger than the ongoing SFR in Mrk 231. Based on kinetic power arguments, we also suggested that the molecular outflow is primarily driven by the quasar radiation pressure.

These findings have been further confirmed through the analysis of broad wings of the H α and Na I D absorption line via IFU optical spectroscopy, which have spatially resolved the outflow on the same scales as traced by the CO wings (Rupke & Veilleux 2011). Furthermore, Aalto et al. (2012) recently detected broad wings also in the HCN(1-0), HCO⁺(1-0) and HNC(1-0) emission lines of Mrk 231, which are tracers of high-density molecular gas, and confirmed the extent of the HCN(1-0) broad emission up to 0.7 kpc. They suggested that the molecular outflow in Mrk 231 is clumpy and dominated by the dense phase, with enhanced HCN abundance, which may indicate either the presence of a shocked medium in the outflow and/or a chemistry influenced by the AGN. Although these characteristics make Mrk 231 an exception in the local Universe, they are expected to be quite common at high redshift, where Mrk 231-like objects are thought to play a major role in the formation of present-day, red massive quiescent elliptical galaxies (Hopkins et al. 2008; Cattaneo et al. 2009). Notably, massive molecular outflows have been recently revealed in additional local ULIRGs

through the detection of prominent OH P-Cygni profiles in their far-IR Herschel spectra (Sturm et al. 2011).

In this work we present the analysis of a new set of IRAM PdBI observations of the CO(1-0) and CO(2-1) transitions in Mrk 231. The aim of this study is to improve the previous results achieved by Feruglio et al. (2010), by spatially resolving the molecular outflow with very high significance ($5-11\sigma$). Moreover we combine the CO(1-0) and CO(2-1) emission line data to investigate the physical conditions of the molecular outflowing gas in this unique source.

A $H_0=70.4 \text{ km s}^{-1} \text{ Mpc}^{-1}$, $\Omega_M = 0.27$, $\Omega_\Lambda = 0.73$ cosmology is adopted throughout this work.

2. Observations

Mrk 231 was observed in CO(1-0) and CO(2-1) with the IRAM millimeter-wave interferometer on Plateau de Bure (IRAM PdBI) between June 2009 and November 2010. The CO(2-1) observations presented allow us to investigate the broad wings in Mrk231 for the first time in this transition. The new CO(1-0) instead allows us to improve over the previous Feruglio et al. (2010) observation by increasing significantly the signal on long baselines and, therefore, allowing us to investigate better the extension of the outflow in this transition. Table 1 summarizes the technical information concerning these observations: the CO transition and the corresponding redshifted frequency ($z=0.04217$), the dates of the observations, the array configurations and the number of antennas used, the on-source integration times, the beam sizes and the relevant references.

The data were calibrated by using the CLIC software of the GILDAS package¹. The main flux calibrator at 110.697 GHz was MWC 349, whose flux at this frequency is 1.27 Jy; the principal flux calibrators at 221.210 GHz were instead 0923+392 and 3C84, whose fluxes at this frequency are 3.11 Jy and 7.71 Jy, respectively. The absolute flux calibration obtained is typically precise to better than 10% at 110.697 GHz and $\sim 20\%$ at 221.210 GHz (Castro-Carrizo & Neri 2010). After calibration, old (2009) and new (2010) data of the CO(1-0) emission line were merged together.

Both the narrow-band and the wide-band (WideX) correlators offered by the PdBI were exploited in our measurements. The WideX provides a spectral resolution of 1.95 MHz over its full bandwidth of 3.6 GHz and it is available in parallel to the narrow-band correlator. The narrow-band correlator, whose maximum signal bandwidth is 2 GHz, was configured to have a spectral resolution of 2.5 MHz. We rebinned the uv-tables obtained with the narrow-band correlator to give frequency channels of 12.5 MHz for CO(1-0) and of 25 MHz for CO(2-1). The wide-band data, thanks to the larger number of line-free channels available, were exploited to produce uv-tables of the continuum emission (sampled from channels with velocities $|v| > 1200 \text{ km s}^{-1}$), which was then subtracted from both the CO(1-0) and CO(2-1) narrow-band and Widex data.

Data imaging, cleaning and analysis were performed using the MAPPING software, also included in the GILDAS package. The field of view of the maps is $2.7 \times 2.7 \text{ arcmin}^2$ at 110.697 GHz and $1.3 \times 1.3 \text{ arcmin}^2$ at 221.210 GHz. We extracted the CO(1-0) and CO(2-1) spectra from the cleaned and continuum-subtracted narrow-band data cubes with an aperture with diameter of 6 arcseconds. The noise levels per channel of the CO(1-0) and CO(2-1) spectra are 0.4 mJy and 1.2 mJy, respectively. We verified that

¹ <http://www.iram.fr/IRAMFR/GILDAS>

Table 1: Properties of the IRAM PdBI CO observations

Line (freq.)	Date(s)	Conf. (no. of ant.)	On source time	Beam (arcsec)	Ref.
CO(1-0) (110.607 GHz)	June-Nov. 09	C+D (5 ant.)	20 hrs	3.2×2.8	Feruglio et al. 2010
	Oct. 10	C (5/6 ant.)	7.4 hrs		This work
CO(2-1) (221.210 GHz)	Sep.-Nov. 10	C+D (5/6 ant.)	4.2 hrs	1.6×1.3	This work

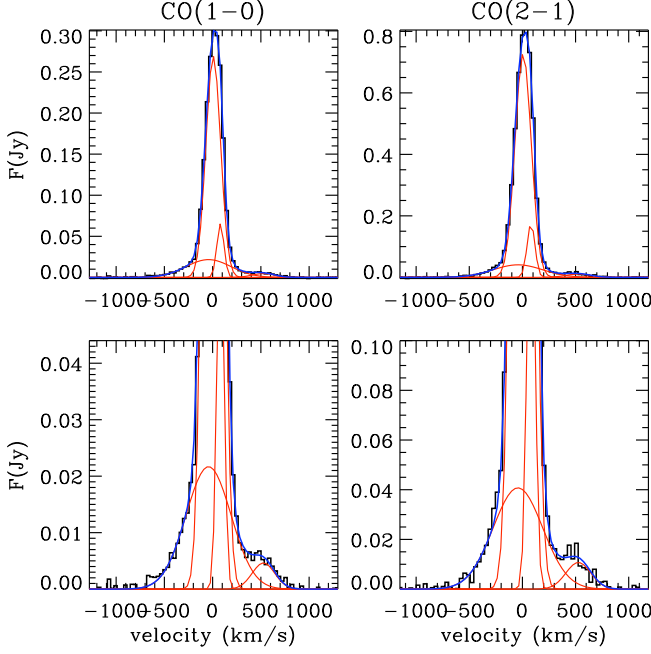


Figure 1: Continuum-subtracted IRAM PdBI spectra of the CO(1-0) and CO(2-1) emission lines. These spectra are extracted from circular apertures with diameter of 6 arcseconds. *Top panels*: full flux scale. *Bottom panels*: expanded flux scale to highlight the broad components. The two emission lines were simultaneously fitted with four Gaussian functions (red profiles, see text), tied to have the same centers and widths for the two transitions, to reproduce the three main components of each line (i.e. core, blue and red broad components). The blue contours represent the results of the fit.

the noise distribution is Gaussian by analysing the distribution histogram of the fluxes.

3. Results

Figure 1 shows the IRAM PdBI spectra of the CO(1-0) and CO(2-1) emission lines extracted from an aperture of 6 arcsec. The broad component, discovered in the (1-0) transition by Feruglio et al. (2010) is clearly present also in the (2-1) transition. The spectra in Figure 1 are fitted by using two narrow Gaussians to fit the core of the CO lines and two broad Gaussians to fit the wings. The centers and widths of the components are linked to be identical for the two CO transitions, but their relative strengths are allowed to vary. The need to use two narrow Gaussians to fit the core probably reflects the gas distribution in the central rotating disk that cannot be described through a simple, single Gaussian.

Table 2: Integrated fluxes

Fluxes from uvfits in velocity intervals				
	Velocity range (km s ⁻¹)	CO(1-0) (Jy km s ⁻¹)	CO(2-1) (Jy km s ⁻¹)	
Narrow core	(-300 ÷ 300)	(64.39 ± 0.13)	(194.00 ± 0.50)	
Blue wing	(-1000 ÷ -400)	(1.84 ± 0.16)	(3.90 ± 0.38)	
Red wing	(400 ÷ 1000)	(2.32 ± 0.17)	(7.08 ± 0.84)	
Total flux	(-1000 ÷ 1000)	(75.98 ± 0.22)	(241.32 ± 0.66)	
Fluxes of Gaussian components				
Component	Velocity (km s ⁻¹)	FWHM (km s ⁻¹)	CO(1-0) (Jy km s ⁻¹)	CO(2-1) (Jy km s ⁻¹)
Narrow core [†]	(6.5 ± 2.0) (80.9 ± 1.3)	(179.7 ± 2.6) (86.3 ± 5.3)	(54.6 ± 1.1)	(173.2 ± 3.3)
Bluer comp.	(-42 ± 16)	(548 ± 35)	(24.9 ± 2.5)	(52.7 ± 6.6)
Redder comp.	(527 ± 30)	(276 ± 71)	(1.96 ± 0.43)	(6.1 ± 1.4)
Total flux			(75.7 ± 1.9)	(240.7 ± 5.6)

Notes: Note that a flux calibration systematic error equal to the 10% of the flux value should be added in quadrature to the statistical error reported with each flux measurement in the table.

[†] The FWHM and the velocity of both the Gaussians fitting the narrow core are reported.

The fluxes extracted from the cleaned cubes may be affected by various uncertainties associated with the cleaning process and aperture effects. Therefore, to estimate rigorously the fluxes of the components, we have used the fluxes inferred directly from the visibility data, which are not affected by any cleaning problem. More specifically, we measure the flux through the uv amplitudes at the 25m baseline. At this baseline the beam width is 14 arcsec at 230 GHz, and it is even larger at lower frequencies: this will therefore ensure that all of the flux in the wings (which are much less extended, as discussed below) is accounted for. To obtain this information we extracted, for both the CO transitions, the amplitude uv diagrams of each spectral line component separately, by averaging the frequency channels corresponding to $-300 \lesssim v(\text{km s}^{-1}) \lesssim 300$ (line core), $-1000 \lesssim v(\text{km s}^{-1}) \lesssim -400$ (blue wing) and $400 \lesssim v(\text{km s}^{-1}) \lesssim 1000$ (red wing). Note that all the three components are continuum-subtracted. In addition, for the visibilities of the narrow core, we also subtracted the contribution of the “near” wings estimated within $-600 \lesssim v(\text{km s}^{-1}) \lesssim -400$ and $400 \lesssim v(\text{km s}^{-1}) \lesssim 600$. In Table 2 we report the fluxes of the CO lines, integrated within these velocity intervals in the uv-amplitude data, along with the total line fluxes estimated within $-1000 \lesssim v(\text{km s}^{-1}) \lesssim 1000$, by applying the same method². The wings are detected at a confidence level ranging from 8σ to 14σ , depending on the transition.

The FWHMs, the velocities and the fluxes of the Gaussian components resulting from the fit shown in Figure 1, are reported in Table 2 as well. The fluxes of the Gaussian components were corrected for aperture and cleaning effects by rescaling their fluxes to the values obtained from the uv-amplitudes in the following way: we integrated the spectra shown in Figure 1 in the same velocity intervals as those used for the uv-amplitudes of the narrow core and the broad wings, and then we estimated the three different scaling factors from the ratios between the fluxes

² Note that the errors reported in Table 2 refer to the statistical errors only. This is what required for inferring the statistical significance and for comparing the relative intensity of the various components within the same transition. However, when comparing with other observations or among different transitions, a systematic error of 10% on the absolute calibration should be added in quadrature.

resulting from the uv-amplitudes and the fluxes obtained by integrating the spectra of the individual Gaussian components. Note that the scaling factors obtained for the broad wings are slightly higher than those obtained for the narrow core, since the spectra extracted from an aperture with a diameter of only 6 arcsec miss part of the broad and faint components of the two CO emission lines.

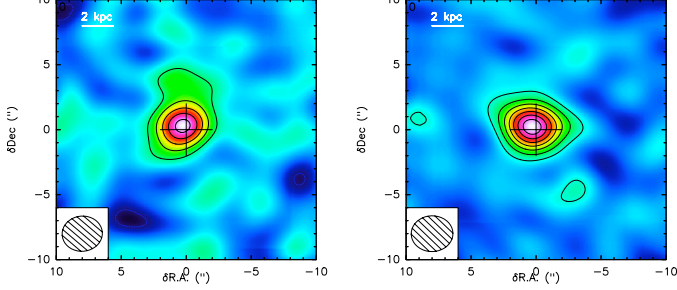


Figure 2: IRAM PdBI maps of the CO(1-0) blue (*left panel*) and red (*right panel*) broad wings. The size of the map is 20×20 arcseconds. Contours correspond to 3σ ($1\sigma = 0.14 \text{ mJy beam}^{-1}$). The synthesized beam size is shown at the bottom of the maps. The cross indicates the peak of the radio (VLBI) emission. Note that the peaks of the wing maps appear to be slightly offset to the peak of the radio VLBI but well within the beam.

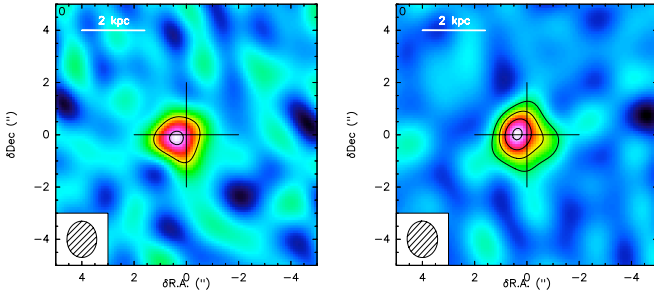


Figure 3: IRAM PdBI maps of the CO(2-1) blue (*left panel*) and red (*right panel*) broad wings. The size of the map is 10×10 arcseconds. Contours correspond to 3σ ($1\sigma = 0.6 \text{ mJy beam}^{-1}$). The synthesized beam size is shown at the bottom of the maps. The cross indicates the peak of the radio (VLBI) emission. A tapering with $uv \text{ taper} = 50 \text{ m}$ has been applied to both the maps; the tapering cuts the visibilities with $uv \text{ radius} < 50 \text{ m}$, so the maps appear more detailed and the synthesized beam is slightly smaller than in the original maps. Note that the peaks of the wing maps appear to be slightly offset to the peak of the radio VLBI but well within the beam.

Figures 2 and 3 show the maps of the blue and red wings of the CO(1-0) and CO(2-1) emission lines and the half-power contours of the synthesized beams. The emission from both the broad components of the CO(1-0) and CO(2-1) lines is spatially resolved. The peaks of the red and blue wings of both the CO(1-0) and the CO(2-1) emission lines are not spatially offset from one another. This validates the hypothesis that these high-velocity components are due to the motion of outflowing gas, roughly in an axisymmetric way relative to the line of sight, instead of a rotating molecular disk. The fact that a large fraction of the outflow occurs along our line of sight is supported by the

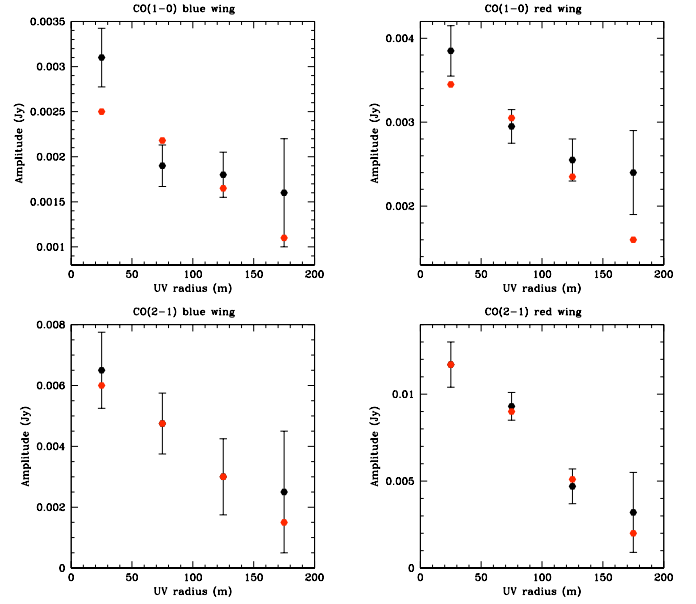


Figure 4: Amplitude of visibilities (Jy) plotted as a function of the uv radius for the blue and red wings of the CO(1-0) and CO(2-1) emission lines (black points with errorbars). The visibilities were binned using intervals of 50 m of uv radius, covering baselines from 10 m to 200 m. The emission from the wings was estimated within the velocity intervals $-1000 \lesssim v(\text{km s}^{-1}) \lesssim -400$ and $400 \lesssim v(\text{km s}^{-1}) \lesssim 1000$. We recall that for a point (i.e. unresolved) source the visibility amplitude would be a constant function of the uv radius. The red points are the results of the best fits with a circular Gaussian model.

blueshifted OH absorption observed in the Herschel PACS spectrum (Fischer et al. 2010).

To quantify the extension of the wings, in Figure 4 we show the amplitude of the visibilities plotted as a function of the uv radius for both the blue and red wings of the CO(1-0) and CO(2-1) emission lines. We binned the visibilities in baseline steps of 50 m. The plots in Figure 4 were fitted with both a point (unresolved) source model and a circular Gaussian source model. The resulting reduced χ^2 and the associated probability P values of the best fits are reported in Table 3, which also gives the differences $\Delta\chi^2 = \chi^2(\text{Point}) - \chi^2(\text{Gaussian})$ and their associated $1 - P$. We estimate the physical extent of the outflow in terms of full width at half maximum (FWHM) resulting from the circular Gaussian model fits to the uv data. Note that since we are fitting directly the uv data, the fit automatically takes into account the interferometric beam size. The resulting sizes are reported in Table 3.

The results in Table 3 demonstrate that both the red and blue wings of the CO(1-0) and of the CO(2-1) lines are spatially resolved at high level of significance (much higher than previously reported in Feruglio et al. 2010 for the CO(1-0) thanks to the higher signal on long baselines even for this transition). More specifically, the spatial distribution of the wings is resolved with a confidence ranging from 5σ to 11σ , depending on the transition and on the wing component. These results prove that the outflow extends out to the kpc scale: FWHM $\sim 1.2 \text{ kpc}$ in the case of the CO(1-0) transition and FWHM $\sim 0.8 \text{ kpc}$ for the CO(2-1) transition.

Summarizing, our new data not only detect for the first time broad wings of the the CO(2-1) transition, and resolve them spa-

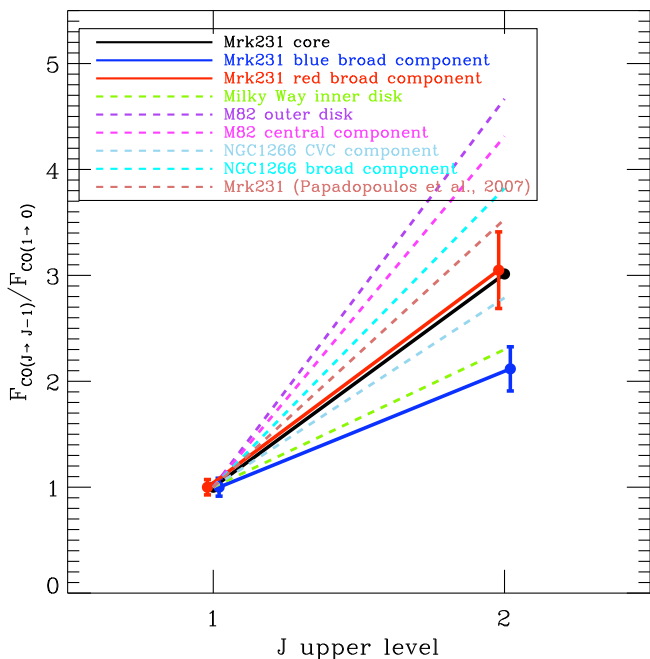


Figure 5: Relative strengths of both the narrow core (*black*) and the broad wings (*blue* and *red*) of Mrk 231’s CO emission lines. The ratios of the CO integrated fluxes were calculated using the data reported in the upper part of Table 2. The CO spectral line energy distribution (SLED) of Mrk 231 obtained by Papadopoulos et al. (2007) is shown for comparison, along with the CO SLEDs of the Milky Way (Fixsen et al. 1999), M82 (Weiß et al. 2005) and NGC1266 (Alatalo et al. 2011).

tially, but also allow us to estimate the extension of the CO(1-0) broad wings with much higher accuracy with respect to previous results (Feruglio et al. 2010).

4. Discussion

4.1. The CO(2-1)/CO(1-0) outflow excitation ratio

The physical conditions of molecular gas in galaxies, such as its kinetic temperature, volume density and optical depth, can be derived from the CO excitation properties and, in particular, from the relative strengths of the CO emission lines. The physical conditions of the molecular gas responsible for the *narrow* components of Mrk 231’s CO emission lines have been widely investigated. Papadopoulos et al. (2007) and van der Werf et al. (2010) found that the rotational excitation diagram of the narrow core of Mrk 231’s CO lines is dominated, in the lower J levels ($J_{upper} \in [1, 3]$), by a component with density $n(\text{H}_2) \sim 10^3 \text{ cm}^{-3}$ and excitation temperature $T \in [55, 95] \text{ K}$. In principle, a similar analysis could be undertaken for the CO wings tracing the outflow. However, two CO transitions are certainly not enough to investigate the excitation and physical conditions of the outflowing gas. As a consequence, in the following we simply compare the CO(1-0)/CO(2-1) ratio observed in the wings with the same ratio observed in the core of the line and with other environments.

Figure 5 shows the CO(1-0)/CO(2-1) ratio for the two wings and for the line core, compared with CO SLEDs observed in other galaxies, more specifically: the Milky Way’s inner disk ($2.5 < |l| < 32.5$) (Fixsen et al. 1999), the outer disk and the central component of M82 (Weiß et al. 2005), both the core and the

broad component of NGC1266 (Alatalo et al. 2011), and the CO core SLED of Mrk 231 obtained by Papadopoulos et al. (2007). Note that the error bars in Figure 5 represent only the statistical uncertainties, since here we are primarily interested in the excitation of the wings relative to the core (hence absolute calibration uncertainties are unimportant). However, when comparing excitation ratios with other targets an uncertainty of 10% should be added in quadrature.

The CO(1-0)/CO(2-1) ratios observed in the red wing and in the narrow core are consistent with each other. The blue wing is less excited than the core of the line. Taken at face value, this result does not support those AGN feedback models where the outflow is generated by a radiation driven shock (“blast wave models”) that, besides accelerating the ISM, should greatly increase its temperature and density (e.g. Lapi et al. 2005; Zubovas & King 2012). However, it is possible that a high excitation component of the outflow may be revealed by high-J transitions. Therefore, sensitive and wide band observations of higher CO transitions are required to further investigate this issue.

However, it should be noted that, since the CO(2-1) wings are more compact than the CO(1-0) wings, the CO(2-1)/CO(1-0) ratio is likely to change radially. More specifically, the CO(2-1)/CO(1-0) ratio should be higher in the central region than in the outer region. Higher angular resolution maps would be required to properly map the CO(2-1)/CO(1-0) ratio and disentangle beam smearing effects. However, based on the circular Gaussian modelling of the spatial distribution of the two wings in the two transitions, we have estimated that within the central 0.7 kpc (FWHM of the blue wing) the CO(2-1)/CO(1-0) ratio of the blue wing increases to 3.5 ± 0.8 , which is however still consistent with the excitation observed in the core of the lines ($F_{\text{CO}(2-1)}/F_{\text{CO}(1-0)} = 2.9$). The CO(2-1)/CO(1-0) flux ratio of the red wing increases in the same inner region to 4.0 ± 0.8 , which starts to be inconsistent with the excitation in the core of the line, although marginally. On the other hand, in the region outside the central 0.7 kpc the CO(2-1)/CO(1-0) ratio drops significantly, below 2, well below the excitation observed in the core of the line. Summarizing, the outflowing gas associated with the blue wing does not show any evidence for higher excitation relative to the core of the line, both globally and even in the central region, indicating that this outflowing gas is not affected by shocks. Within the central region the gas associated with the red wing does show marginally higher excitation, suggesting that this component of the outflowing gas may be affected by some shocks.

The high Mach number inferred by Feruglio et al. (2010), based on the outflow velocity of the molecular clouds, would also suggest the presence of shocks. However, we also note that high outflow velocities do not necessarily translate into a large Mach number, since the medium embedding the clouds may be outflowing with the same velocity (as it appears to be the case from the similar velocity of the ionized gas found by Rupke & Veilleux 2011), hence resulting in little differential velocity between the molecular clouds and the surrounding gas.

Another important implication of our result is that the CO-to-H₂ conversion factor in the wings may not be too different with respect to the bulk of the gas in the host galaxy traced by the narrow CO component (i.e. a ULIRG-like conversion factor). In Feruglio et al. (2010) we had been conservative by assuming, for the outflow, a conversion factor $\alpha = 0.5 M_{\odot} (\text{K km s}^{-1} \text{pc}^2)^{-1}$ (i.e. 1/10 of the Galactic value and 40% lower than the value assumed for ULIRGs); this is the lowest conversion factor found in different locations of M82, including its molecular outflow

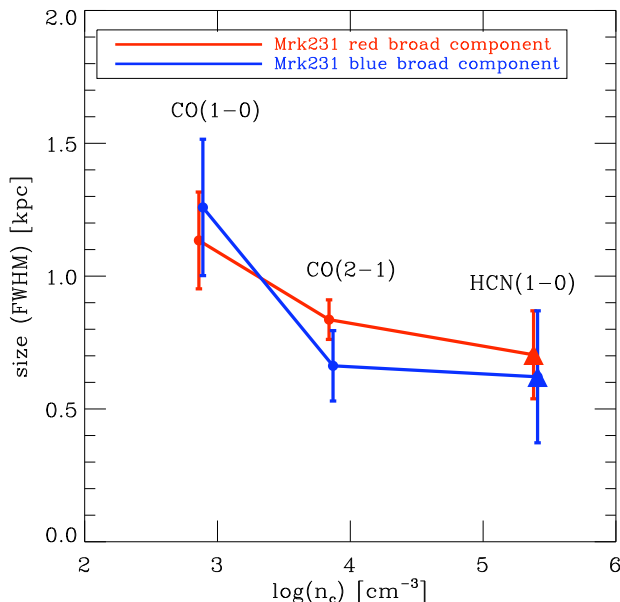


Figure 6: Size (FWHM) of the outflow plotted as a function of the critical density of the corresponding molecular transition used as a wind tracer. Our CO(1-0) and CO(2-1) IRAM PdBI data are represented by filled circles, while the HCN(1-0) observations by Aalto et al. (2012) are denoted by filled triangles. Critical densities were calculated for a molecular medium at $T = 100$ K. Note that the same conversion factor of 0.828 kpc arcsec^{-1} has been applied to all data in order to allow comparisons.

(Weiß et al. 2001). The finding that the CO excitation in the outflow is not significantly different (or even lower) relative to the core of the line, tracing the bulk of the gas in this ULIRGs, suggests that the conversion factor is also similar (i.e. $\alpha = 0.8 M_{\odot} (\text{K km s}^{-1} \text{pc}^2)^{-1}$). This implies that the outflow molecular mass and outflow rate given in Feruglio et al. (2010) are significantly underestimated, and are probably higher by a factor of about 1.4.

We note that in the jet-driven outflow observed in NGC 1266 by Alatalo et al. (2011) the excitation of the CO broad components tends to be higher than in the Central Velocity Component (as illustrated in Fig. 5), although not strongly. This is not unexpected. Indeed, in this case, the outflow is totally driven by jet-induced shocks, which unavoidably heat the ISM and therefore produce higher CO excitation. The outflow CO excitation differences between Mrk 231 and NGC 1266 further highlight that the driving mechanism in the two sources are different, although both associated with an AGN.

Finally, we note that the Mrk 231 SLED of the core obtained by Papadopoulos et al. (2007) through single dish observations is slightly steeper than the one obtained by us. We ascribe the difference partly to calibration uncertainties and partly to uncertainties in subtracting the continuum and broad wings with previous narrow band spectra (especially in single dish data where the baseline instabilities may be problematic).

4.2. Extension of the outflow

As mentioned above, our new data have allowed us to constrain the size of the molecular outflow traced by the CO transitions with unprecedented accuracy, enabling analyses that were not possible until now. The results presented in the previous sec-

tion clearly reveal that the extension of the outflow traced by the CO(1-0) transition is significantly larger than observed in the CO(2-1) and HCN(1-0) transitions. Fig. 6 shows the extension of the outflow as a function of the critical density of the transition used to trace the outflow, where the red and blue symbols indicate the trends relative to the red and blue wings, respectively. There is a clear trend for the size of the outflow to decrease as a function of the critical density, at least between $10^3 < n_{\text{cr}} < 10^4 \text{ cm}^{-3}$ (while at higher densities it is more difficult to assess this trend due to the large errorbars on the size of the HCN wings).

A radial decreasing density of the outflowing molecular gas is also consistent with the Herschel measurements by Fischer et al. (2010) and Sturm et al. (2011), and in particular with the blueshifted absorption profile of the far-IR molecular transitions observed in the PACS spectra (OH $79\mu\text{m}$, OH $119\mu\text{m}$, ^{18}OH $120\mu\text{m}$, H $_2\text{O}$ $79\mu\text{m}$), as discussed in those papers.

This result is consistent with the prediction by Narayanan et al. (2008), who studied the response of CO morphology to starburst and AGN feedback-driven winds in galaxy mergers. According to them, the emission from higher CO transitions (e.g. CO(2-1)) broadly follows the distribution of the CO(1-0) emission, but remains slightly more compact. This is due to the fact that, according to their model, denser clouds (preferentially traced by higher transitions) have shorter lifetime along the outflow and tend to evaporate into a more diffuse molecular phase, traced by the CO(1-0) transition.

The result could also possibly support the scenario proposed by Hopkins & Elvis (2010), where dense clouds invested by an even mild AGN-driven wind develop Kelvin-Helmholtz instabilities making them expand and easier to accelerate by radiation pressure. In the latter scenario one would expect diffuse clouds to be driven to larger distances relative to the denser clouds. However, Kelvin-Helmholtz instabilities should also develop shocks (although much milder than those expected in “blast wave models”), that should show up in higher gas excitation, which is not the case for the blue wing, while it may apply to the red wing.

Simple acceleration by radiation pressure on the dust in molecular clouds (Fabian et al. 2009), without invoking any scenario associated with shocks, may explain not only the modest CO excitation in the wings, but also the size difference between CO(1-0) and CO(2-1)+HCN emission. Indeed, more diffuse clouds (preferentially traced by CO(1-0)) are characterized by a higher ratio between outward radiation pressure and inward gravitational pull than dense clouds (preferentially traced by CO(2-1)+HCN emission). More specifically, for clouds whose dust is optically thick to UV/optical radiation, the ratio $F_{\text{rad}}/F_{\text{grav}}$ is inversely proportional to the column density of the cloud N_{H} (which is higher in dense clouds). As a consequence, diffuse clouds can be expelled to larger distances.

So far we have discussed only the global size of the emitting regions of the two CO transitions obtained by fitting the uv data with a simple circular Gaussian. At our resolution the maps do not show much structure. Possibly the only relevant structure at the 3σ level is an extension of the CO(1-0) blue wing (Fig. 2, left) a few arcseconds to the North. This could imply an association between some of the molecular outflow (a minor part of it) and the northern region, where the radio jet is affecting the neutral gas outflow as inferred by Rupke & Veilleux (2011) through the blueshifted Na I D kinematics map. Aalto et al. (2012) detect a plum extending to the North in the HCN(1-0) red-shifted wing map and also infer a link between this feature and the jet-influenced neutral wind detected by Rupke & Veilleux (2011).

Table 3: Best fit results of the visibility vs uv radius plots.

Line	Velocity range (km s ⁻¹)	Point source model	Gaussian source model	$\Delta\chi^{2\dagger}$	FWHM (arcsec)	FWHM \ddagger (kpc)
CO(1-0) blue wing	(-1000 ÷ -400)	$\chi_r^2 = 4.14$ $P = 6.1E-03$	$\chi_r^2 = 1.98$ $P = 0.11$	$\Delta\chi^2 = 6.48$ (1 - P) = 0.99	(1.52 ± 0.31)	(1.26 ± 0.25)
CO(1-0) red wing	(400 ÷ 1000)	$\chi_r^2 = 4.26$ $P = 5.2E-03$	$\chi_r^2 = 1.74$ $P = 0.16$	$\Delta\chi^2 = 7.54$ (1 - P) = 0.99	(1.37 ± 0.22)	(1.13 ± 0.18)
CO(2-1) blue wing	(-1000 ÷ -400)	$\chi_r^2 = 1.69$ $P = 0.17$	$\chi_r^2 = 0.14$ $P = 0.94$	$\Delta\chi^2 = 4.65$ (1 - P) = 0.97	(0.80 ± 0.16)	(0.66 ± 0.14)
CO(2-1) red wing	(400 ÷ 1000)	$\chi_r^2 = 8.94$ $P = 6.5E-06$	$\chi_r^2 = 0.19$ $P = 0.90$	$\Delta\chi^2 = 26.24$ (1 - P) ≈ 1.00	(1.01 ± 0.09)	(0.84 ± 0.07)

Notes: [†] $\Delta\chi^2 = \chi^2(\text{Point}) - \chi^2(\text{Gaussian})$ [‡] The adopted cosmology and redshift result in a spatial scale of 0.828 kpc arcsec⁻¹.

However, we do not think this association is correct, since the jet-accelerated gas is detected through *blueshifted* Na I D absorption, so any association should be seen with the molecular *blue* wings, not with the red wings. The possible interaction between some of the molecular outflow and the radio-jet must however be investigated through higher-resolution data.

Finally, we note that the size (~2 arcsec) of the (blueshifted) “nuclear wind”, which is the region identified by Rupke & Veilleux (2011) where the outflow is dominated by a radiation-pressure drive wind, is close to the size (1.5 ± 0.3 arcsec) of the molecular outflow determined by us from the blue wing of the CO(1-0) component.

5. Conclusions

We have presented new broad band IRAM PdBI observations of the CO(2-1) transition in Mrk 231, the ULIRG hosting the closest quasar known. The observations reveal for the first time broad wings of the (2-1) transition, extending to velocities of FWZI~1500 km s⁻¹, which trace the same molecular wind revealed by previous CO(1-0) PdBI observations and PACS far-IR spectroscopy of OH transitions. The CO(2-1) wings are spatially resolved, with an extension of about 0.8 kpc.

We also obtain new CO(1-0) observations, by improving significantly the signal at high angular resolution relative to previous works, that allow us to better determine the size of the molecular outflow traced by this transition. The CO(1-0) broad wings are spatially resolved with a significance much higher (5–7 σ) than in previous observations. We measure an extension of the CO(1-0) wings of about 1.2 kpc, significantly larger than observed for the CO(2-1) wings. The extension of the CO(1-0) wings is also significantly larger than the extension of the HCN(1-0) wings, tracing high density gas in the outflow, obtained by previous observations. More specifically, we show that the size of the outflow anticorrelates with the critical density of the transitions used to trace the outflow.

These results are consistent with the scenario where denser clouds (traced by the CO(2-1) and HCN(1-0) broad wings) have shorter lifetime along the outflow and evaporate into a more diffuse molecular component (traced by CO(1-0)) at larger radii, as predicted by some feedback models.

We also find that the CO excitation in the outflow, as traced by the CO(2-1)/CO(1-0) ratio of the broad wings, is not significantly different with respect to the gas in the bulk of the galaxy, as traced by core of the CO lines. Actually, in the blue

wing the excitation is lower than in the core of the line. Taken at face value, this result does not support those models where the molecular outflow is driven by a shock wave generated by the interaction of a radiation pressure-driven nuclear wind with the ISM of the host galaxy. We favor a scenario where gas clouds are directly accelerated by the radiation pressure on dust. This scenario does not need to invoke shocks, hence the CO excitation is not affected. Moreover, in this scenario low density clouds (traced by CO(1-0)) are accelerated more efficiently, hence reaching larger distances relative to dense clouds (traced by CO(2-1) and HCN). However, we also note that in the inner region (R < 0.3 kpc) the CO(2-1)/CO(1-0) ratio is indeed slightly higher, possibly suggesting some shock contribution.

We marginally detect an extension of the CO(1-0) blueshifted wing to the North, where previous studies have found evidence for the atomic neutral outflow, traced by blueshifted Na I D absorption, being influenced by the radio-jet. This suggests that the radio jet may also contribute to the acceleration of some of the molecular outflow, although a minor fraction with respect to the global molecular outflow.

Acknowledgements. We thank Andrea Lapi for helpful suggestions and discussions. We are grateful to the IRAM staff in Grenoble for helping with data reduction and calibration.

This work is based on observations carried out with the IRAM Plateau de Bure Interferometer. IRAM is supported by INSU/CNRS (France), MPG (Germany) and IGN (Spain). This work was supported by ASI/INAF contract I/009/10/0.

References

- Aalto, S., Garcia-Burillo, S., Muller, S., et al. 2012, *Astronomy and Astrophysics*, 537, A44
- Alatalo, K., Blitz, L., Young, L. M., et al. 2011, *The Astrophysical Journal*, 735, 88
- Alexander, D. M., Swinbank, A. M., Smail, I., McDermid, R., & Nesvadba, N. P. H. 2010, *Monthly Notices of the Royal Astronomical Society*, 402, 2211
- Baldry, I. K., Balogh, M. L., Bower, R., Glazebrook, K., & Nichol, R. C. 2004, in *American Institute of Physics Conference Series*, Vol. 743, *The New Cosmology: Conference on Strings and Cosmology*, ed. R. E. Allen, D. V. Nanopoulos, & C. N. Pope, 106–119
- Boroson, T. A. & Meyers, K. A. 1992, *The Astrophysical Journal*, 397, 442
- Braito, V., Della Ceca, R., Piconcelli, E., et al. 2004, *Astronomy and Astrophysics*, 420, 79
- Cano-Díaz, M., Maiolino, R., Marconi, A., et al. 2012, *Astronomy and Astrophysics*, 537, L8
- Castro-Carrizo, A. & Neri, R. 2010, *IRAM Plateau de Bure Interferometer Data Reduction Cookbook*
- Cattaneo, A., Faber, S. M., Binney, J., et al. 2009, *Nature*, 460, 213
- Croton, D. J., Springel, V., White, S. D. M., et al. 2006, *Monthly Notices of the Royal Astronomical Society*, 365, 11

- Davies, R. I., Tacconi, L. J., & Genzel, R. 2004, *The Astrophysical Journal*, 613, 781
- Di Matteo, T., Springel, V., & Hernquist, L. 2005, *Nature*, 433, 604
- Elvis, M. 2006, *Memorie della Societ Astronomica Italiana*, 77, 573
- Fabian, A. C. 1999, *MNRAS*, 308, L39
- Fabian, A. C. 2012, *ArXiv e-prints*
- Fabian, A. C., Celotti, A., & Erlund, M. C. 2006, *Monthly Notices of the Royal Astronomical Society*, 373, L16
- Fabian, A. C., Vasudevan, R. V., Mushotzky, R. F., Winter, L. M., & Reynolds, C. S. 2009, *Monthly Notices of the Royal Astronomical Society*, 394, L89
- Farrah, D., Urrutia, T., Lacy, M., et al. 2012, *The Astrophysical Journal*, 745, 178
- Ferrarese, L. & Ford, H. 2005, *Space Science Reviews*, 116, 523
- Feruglio, C., Maiolino, R., Piconcelli, E., et al. 2010, *Astronomy and Astrophysics*, 518, L155+
- Fischer, J., Sturm, E., González-Alfonso, E., et al. 2010, *Astronomy and Astrophysics*, 518, L41+
- Fixsen, D. J., Bennett, C. L., & Mather, J. C. 1999, *The Astrophysical Journal*, 526, 207
- Granato, G. L., De Zotti, G., Silva, L., Bressan, A., & Danese, L. 2004, *The Astrophysical Journal*, 600, 580
- Greene, J. E., Zakamska, N. L., Ho, L. C., & Barth, A. J. 2011, *The Astrophysical Journal*, 732, 9
- Gültekin, K., Richstone, D. O., Gebhardt, K., et al. 2009, *The Astrophysical Journal*, 698, 198
- Hopkins, P. F., Cox, T. J., Kereš, D., & Hernquist, L. 2008, *The Astrophysical Journal Supplement Series*, 175, 390
- Hopkins, P. F. & Elvis, M. 2010, *Monthly Notices of the Royal Astronomical Society*, 401, 7
- King, A. 2005, *The Astrophysical Journal*, 635, L121
- King, A. R. 2010, *MNRAS*, 402, 1516
- King, A. R. & Pounds, K. A. 2003, *Monthly Notices of the Royal Astronomical Society*, 345, 657
- Lapi, A., Cavaliere, A., & Menci, N. 2005, *The Astrophysical Journal*, 619, 60
- Lipari, S., Sanchez, S. F., Bergmann, M., et al. 2009, *Monthly Notices of the Royal Astronomical Society*, 392, 1295
- Maiolino, R., Gallerani, S., Neri, R., et al. 2012, *arXiv:1204.2904*
- Marconi, A. & Hunt, L. K. 2003, *The Astrophysical Journal*, 589, L21
- Menci, N., Fiore, F., Puccetti, S., & Cavaliere, A. 2008, *The Astrophysical Journal*, 686, 219
- Menci, N., Fontana, A., Giallongo, E., Grazian, A., & Salimbeni, S. 2006, *The Astrophysical Journal*, 647, 753
- Narayanan, D., Cox, T. J., Kelly, B., et al. 2008, *The Astrophysical Journal Supplement Series*, 176, 331
- Nesvadba, N. P. H., Boulanger, F., Salomé, P., et al. 2010, *Astronomy and Astrophysics*, 521, A65
- Nesvadba, N. P. H., Polletta, M., Lehnert, M. D., et al. 2011, *Monthly Notices of the Royal Astronomical Society*, 415, 2359
- Papadopoulos, P. P., Isaak, K. G., & van der Werf, P. P. 2007, *The Astrophysical Journal*, 668, 815
- Rupke, D. S. N. & Veilleux, S. 2011, *The Astrophysical Journal*, 729, L27+
- Sanders, D. B., Mazzarella, J. M., Kim, D.-C., Surace, J. A., & Soifer, B. T. 2003, *The Astronomical Journal*, 126, 1607
- Silk, J. & Rees, M. J. 1998, *Astronomy and Astrophysics*, 331, L1
- Sturm, E., González-Alfonso, E., Veilleux, S., et al. 2011, *The Astrophysical Journal*, 733, L16+
- Taylor, G. B., Silver, C. S., Ulvestad, J. S., & Carilli, C. L. 1999, *The Astrophysical Journal*, 519, 185
- van der Werf, P. P., Isaak, K. G., Meijerink, R., et al. 2010, *Astronomy and Astrophysics*, 518, L42+
- Weiß, A., Neininger, N., Hüttemeister, S., & Klein, U. 2001, *Astronomy and Astrophysics*, 365, 571
- Weiß, A., Walter, F., & Scoville, N. Z. 2005, *Astronomy and Astrophysics*, 438, 533
- Zubovas, K. & King, A. 2012, *The Astrophysical Journal Letters*, 745, L34